**Proceedings 10th NUMGE 2023**
10th European Conference on Numerical Methods in Geotechnical Engineering
Zdravkovic L, Kontoe S, Taborda DMG, Tsiampousi A (eds)


https://doi.org/10.53243/NUMGE2023-129

# Integrated numerical modelling of soil-anchor-mooring line-floater response for floating offshore wind

K.A. Kwa[1] , O. Festa[1] , D.J. White[1], A. Sobey[1,2] , S. Gourvenec[1]

[1] *Civil, Maritime and Environmental Engineering Department, University of Southampton, Southampton, UK*
[2]*Data-centric Engineering, Alan Turing Institute, London, UK*

**ABSTRACT:** This paper presents the development of an anchor macro model and its integration with mooring analyses, for easy coupling of the anchor-seabed-mooring response and full system modelling of a floating offshore wind turbine. The model combines techniques that (i) mobilise additional seabed resistance by considering the added mass and whole-life effects of changing strength of the seabed and (ii) reduce the anchor loads by considering a compliant mooring system, to result in reduced required anchor size. The benefits of combining these approaches lead to reductions of up to 50 % in the minimum required anchor size for the same system reliability.
**Keywords:** Macro-modelling; Anchors; Offshore Geotechnics; Whole-life modelling;

## 1 INTRODUCTION

### *1.1 Background and Aim*

Floating offshore wind (FOW) infrastructure is subject to a wide range of actions from metocean and operational conditions, which are transmitted via mooring lines to the anchor. These loads can affect the geotechnical properties of the seabed and in turn affect the capacity and response of the infrastructure over its lifetime (Gourvenec, 2020). However, typical mooring-floater fluid-structure interaction analyses model the connection of the mooring lines to the seabed as a fixed pin connection and so seabed-anchor interactions with the mooring and floater analysis are generally not considered. This uncoupled method of analysis can result in potentially overconservative anchor designs.

This challenge is addressed by using a novel anchor macro model, referred to as *Ancmac*, that captures the 'whole-life' geotechnical response of the seabed surrounding the anchor, and simply and practically connects with mooring analyses. In this context, whole-life geotechnics, enables assessment of the through-life changes in seabed response and anchor capacity as a result of variable mooring tensions that are applied to the anchor over the lifetime of the FOW infrastructure. This approach can have beneficial design outcomes over traditional design methods including more accurate predictions of seabed-anchor response, available anchor capacity and required anchor size throughout the FOW design lifetime. This study describes *Ancmac* and its integration with FOW mooring analyses to demonstrate the benefits of considering the coupled seabed-anchor-mooring floater response over an idealised FOW facility lifetime of 20 years.

## 2 ANCHOR-MOORING-FLOATER MODEL CONFIGURATION

### *2.1 Geotechnical anchor model*

*Ancmac* is a macro model which simulates the response of an anchor in terms of the resultant forces at the anchor, as an idealisation of the integrated effect of the surrounding elements of soil. The approach was formalised in the 1990s by Nova et al. (1991), Houlsby et al. (1992) and Schotman (1989) by using a plasticity framework. The novel contribution of this study is that the anchor strength is a time-varying function of the applied loads, reflecting short term processes of softening and pore pressure generation, $u$, and long-term processes of consolidation where the seabed can also recover, harden and strengthen over the whole-life time. This approach could be incorporated into multi-directional anchor macro models (such as those presented in Cassidy et al. 2012; Peccin da Silva, 2021).

*Ancmac* is explicit, following the terminology of Jostad et al. (2022), as a time history of cyclic anchor loading is converted to increments of the model state parameters. These parameters are then translated into spring-sliders, dashpots and added mass mechanical analogue parameter (MAP) components – which define an extended parallel Iwan model (Iwan, 1967) that represents the anchor in a time domain of the next set of cyclic loads. The updating of the MAPs takes place at intervals that are long enough in time so that the whole operating life of an anchor can be modelled efficiently, but also short enough that the anchor capacity does not change significantly during a single simulated set of cycles. 'Failure' of the embedded anchor is identified when any of the anchor loads that are mobilized exceed the current anchor capacity.

The overall simulation process (as summarised in Figure 1) involves two elements; *Ancmac* and a wrapper

program $K^2M^2$. *Ancmac* holds the current MAP components of the anchor model, which do not change in value during a time domain analysis of mooring lines during a certain sea state. For every time domain analysis of the mooring line, *Ancmac* outputs a series of cyclic anchor forces and the corresponding anchor movements (i.e. displacements, $x$, velocities, $v$, and accelerations, $a$) at the anchor point.

The wrapper program, referred to as $K^2M^2$, uses an acceleration strategy that factors up the number of cyclic loads from *Ancmac* to represent a longer period of time. $K^2M^2$ then uses the upscaled force time series to accumulate the pore pressures or damage applied to the seabed, $D$, from the time history of applied loads from RSN curves, which are based on the mean, $R$, and cyclic amplitude, $S$, of the applied load cycles, $N$ (Verruijt, 1995, Andersen, 2015 and Tom et al., 2019). $K^2M^2$ also handles consolidation and the updating of soil strength and other state parmeters using a critical state inspired (CSI) method as described in White et al., (2021). These are used to update the *Ancmac* spring-slider MAPs before before $K^2M^2$ moves to the next time domain simulation. Therefore, together, *Ancmac* and $K^2M^2$ predict the through-life changes in anchor capacity and movements of the anchor at the anchor point over different time scales and enable easy coupling with mooring-floater analyses which do not traditionally model these aspects. The following sub sections will briefly describe formulation of the MAP model components. The detailed formulation and benchmarking of the model has been presented in separate studies (Kwa et al., 2021b, 2022, 2023).

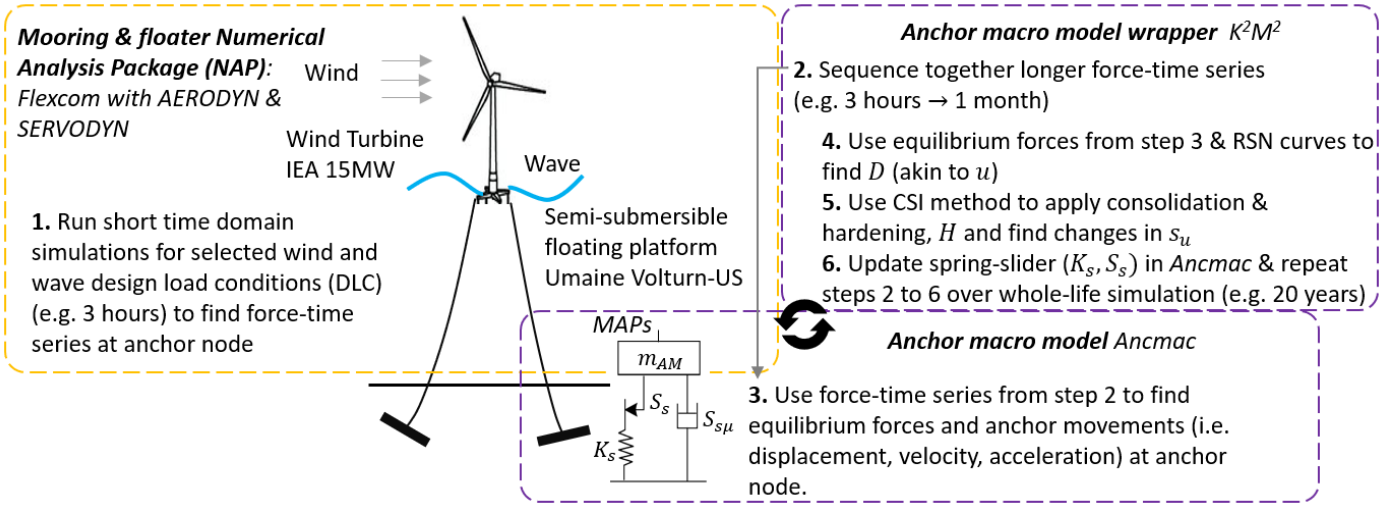


*Figure 1: Anchor-mooring-floater model configuration*

### *2.1.1 Spring-slider component*

A parallel Iwan (PI) model defines the force-displacement responses in *Ancmac*. This consists of a number of spring-slider elements, connected in parallel and defined by parameters $K_{s,}$ and $S_s$. The number of spring, $K_s$, and slider, $S_s$, elements and their initial parameters can be derived from the monotonic backbone curve, as outlined in Kwa et al. (2022, 2023). The force in any spring, $F_{PI,n}$, is the product of the elastic displacement, $\delta_e$, and the spring stiffness, $K_{s.}$ The elastic displacement is the difference between the total displacement, $\delta$, and the plastic displacement, $\delta_p$,

$$F_{PI,i} = K_{s,i}\,(\delta - \delta_p), \tag{1}$$

where if $abs(F_{PI,i}) > K_{s,i}$, the capacity of the slider has been exceeded and the value of the plastic displacement must be incremented by the change in total displacement. Therefore, the resulting force from the spring-sliders is given in equation 2,

$$F_{PI} = min[\textstyle\sum_{j=1}^{i} S_{s,j}\,, \sum_{j=i+1}^{n} K_{s,j}(\delta_j - \delta_{p,j})\,]. \tag{2}$$

During a whole-life analysis, the values of $K_{si}$ or $S_{si}$ are updated in the $K^2M^2$ routine to reflect a whole-life soil response where soil strength and therefore anchor capacity, $Q_s$, can evolve with time due to shearing and consolidation of the soil during sustained and variable low amplitude cyclic loads according to Equation 3;

$$Q_s = f(D, H, \{s_u\}) \tag{3}$$

where $D$ is damage, which leads to a reduction in soil strength and varies by $D = 0 \rightarrow 1$. The damage is calculated using the RSN curves. The hardening, $H$, is also defined such that $H = 0 \rightarrow 1$, and is a result of the dissipation of damage. It reflects the progressive gain in soil strength as the soil densifies. Finally, $\{s_u\}$, is the potential range of undrained soil strengths. Defining $Q_s$ in this manner enables the model to capture rises in the long-term capacity of anchor in a similar manner to established approaches for the capacity of surface foundations and pipelines (e.g. Bransby et al. (2002); Gourvenec et al. (2014); Cocjin et al. (2014); O'Loughlin et al. (2020)). To update $K_{si}$, the model uses non-dimensionalised elastic responses and shear

modulus vs. overconsolidation ratio relationships (Houlsby et al., 1991) as defined in Equation 4;

$$K_{s,i} = G_s \frac{B}{2} K_v, \quad (4)$$

where $B$ is anchor diameter, $K_v$, is a dimensionless elastic stiffness coefficient dependent on the anchor embedment ratio and ν=0.5, in undrained conditions, both of which are assumed to be constant during the analyses. The shear modulus, $G_s$, is given by Equation 5;

$$G_s = \left(\frac{G_s}{s_u}\right)_{nc} (OCR^{\eta-\Lambda} \times s_u), \quad (5)$$

where $\left(\frac{G_s}{s_u}\right)_{nc}$ is the initial shear modulus to undrained strength of a normally consolidated soil, η is a fitting constant, typically taken as 0.5 in clays, Λ depends on the slopes of the normal compression and unloading/reloading lines λ and κ according to the relationship $\Lambda = \frac{\lambda-\kappa}{\lambda}$ and the over consolidation ratio, OCR, is related to hardening, $H$. Therefore, $K_{si}$, changes according to

$$\frac{K_{s,i}}{K_{s,0}} = \frac{OCR_i^{\eta-\Lambda} \times s_{u.i}}{OCR_0^{\eta-\Lambda} \times s_{u.0}}. \quad (6)$$

The slider value, $S_{s,i}$, is related to changes in undrained strength as,

$$S_{s,i} = N_c \, s_u \left(\frac{B}{2}\right)^2 \pi \quad (7)$$

where $N_c$ is the bearing capacity factor and is 13.11 for a deeply embedded a circular rough plate (Martin et al., 2001). Therefore, changes in the slider component are dependent on variations in the undrained strength as $\frac{S_{s,i}}{S_{s,0}} = \frac{s_{u.i}}{s_{u,0}}$.

### 2.1.2 Dashpot component

Viscous rate effects are defined using a dashpot with a resistance proportional to the inverse hyperbolic sine of the strain rate or velocity as defined in (Randolph 2004). This has been used to find modified slider capacities, $S_{s\mu,i}$ to capture increases in undrained strength due to viscous soil effects as defined below.

$$S_{s\mu,i} = S_s \left(1 + \mu' \sinh^{-1} \frac{\dot{\gamma}}{\dot{\gamma_{ref}}}\right) \quad (8)$$

### 2.1.3 Added mass component

Extra dynamic anchor capacity can also be created from mobilising the mass of the soil surrounding the plate under highly dynamic snatch loading conditions (Kwa et al., 2021a). A lumped mass, $m_{AM}$, represents the mass of the anchor and soil around the anchor mobilised and a resistance force associated with having to accelerate this added mass according to Newton's 2nd Law. The added mass term can also be defined by a dimensionless added mass coefficient, $N_{AM}$, which under 2D plane strain and 3D axisymmetric cases are;

$$N_{AM,2D} = \frac{m_{AM}}{\rho B^2}, \; N_{AM,3D} = \frac{m_{AM}}{\rho B^3}, \quad (9)$$

where ρ is the density of the medium. These $N_{AM}$ terms have been analytically determined for plate anchors embedded in soft clays in Kwa et al., (2021a) by using conventional geotechnical collapse mechanisms to derive the geotechnical counterpart to the established added mass solutions derived for fluid flow, and are approximately doubled compared to added mass mobilised in the inviscid fluid case (Table 1).

*Table 1: Geotechnical and fluid inviscid added mass coefficients $N_{AM}$ for embedded plate anchors*

| $N_{AM}$ | Geotechnical | Fluid inviscid flow field |
|---|---|---|
| $N_{AM,2D}$ | 1.678[a], 3.356[b] | 0.785 |
| $N_{AM,3D}$ | 0.548[a], 0.599[b] | 0.333 |

[a] rough, [b] smooth cases

## 2.2 Mooring-floater model

### 2.2.1 Flexcom model of a FOW Turbine

The modelling of the floater, turbine and mooring system was performed using Flexcom, a commercial FEM software. Flexcom offers fully-coupled aero-hydro-servo modelling using FAST plug-ins AERODYN and SERVODYN, and has been validated against other software as part of an offshore code collaboration project OC6 (Robertson et al., 2020). The FOW turbine model used in this study is composed of the International Energy Agency (IEA)15 MW wind turbine and the Umaine Volturn-US semi-submersible floating platform. The full platform and turbine characteristics are described in detail in NREL publications (Evan et al, 2020; Allen et al., 2020).

Two taut mooring configurations are considered (i) a conventional taut mooring system composed of high modulus synthetic polyester rope; and (ii) a taut mooring system, composed of the same polyester rope, with the addition of a polymer spring load reduction device (LRD) at each fairlead. This LRD, based on the Tfi Seaspring (Lozon et al., 2022), can safely operate at high strain (20 - 50%), thus providing high levels of elongation to reduce dynamic loads on mooring lines and anchors. The LRD is modelled with a 3-phase non-linear stiffness curve, to match the curve of the Tfi Seaspring. The general mooring parameters are shown in Table 2, with profile views of both configurations as shown in Figure 3, where the mooring lines are connected to the seafloor via a fixed pin connection.

*Table 2: Mooring parameters for taut mooring systems*

| Parameter | Value |
|---|---|
| Water depth | 150 m |
| Number of mooring lines | 3 |
| Anchor radius from platform centerline | 260 m |
| Seabed-mooring line angle | 34 ° |
| Polymer rope stiffness | 7 MN |
| Polymer rope linear density | 8.5 kg/m |
| Fairlead pre-tension | 2000 kN |

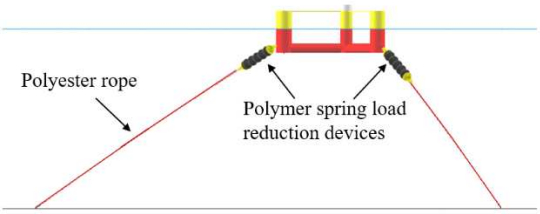


*Figure 2: Profile view of taut mooring with load reduction devices (LRDs). The model of the conventional mooring system does not have the LRDs in the mooring lines.*

### *2.2.2 Applied metocean conditions*

Stochastic load cases were applied to the FOW model based on the IEA design load case (DLC) matrix. From the matrix of load cases, two operational load cases were selected, one above and below the turbine's rated wind speed, as well as the parked turbine cases for a storm and extreme 1-in-50 year storm, as summarised in Table 3.

*Table 3: Summary of design load cases used in this study, selected from UMaine design matrix (Allen et al., 2020)*

| IEA DLC ref. | Load case description | Wind Speed | Sig. wave height | Peak wave period | Shape factor |
|---|---|---|---|---|---|
| 1.1 | Operational Below-rated | 4 m/s | 1.1 m | 8.52 s | 1.00 |
| 1.1 | Operational Above-rated | 12 m/s | 1.84 m | 7.44 s | 1.00 |
| 6.3 | Parked storm | 38 m/s | 6.98 m | 11.70 s | 2.75 |
| 6.1 | 1 in 50 year storm | 47.5 m/s | 10.70 m | 14.20 s | 2.75 |

All environmental loads are applied in the same direction and each simulation is run for 10800 s (3 hours). The resulting force time-series was measured at the point where the windward mooring line attaches to the seafloor and these time-series were used to build synthetic yearly realisations reflecting seasonality in anchor loads in the example whole-life application described in Section 3.

## 3 WHOLE LIFE EXAMPLE APPLICATION

### *3.1 Applied loads on anchor*

In this idealised example application of the anchor-mooring-floater model, the DLC combinations summarised in Table 3 were used to build synthetic anchor load cases, chosen to artificially reflect seasonality of metocean conditions within a year (i.e. calmer in summer and more severe in winter) as shown in Figure 4. This combination of DLCs was repeated over 20-years to idealise a design life time of anchor loads. To investigate the response of the system under an extreme loading event, the 1 in-50-year storm case was applied for a period of 3 hours at year 15 of the design lifetime. It was also assumed that the mooring line tensions were transmitted directly to the anchor. In reality, additional geotechnical resistance from interactions between the embdedded mooring line section and the seabed would reduce the load transmitted to the anchor. Based on analytical solutions for the frictional capacity of embedded anchor chains (Neubecker et al., 1995), this decrease in load would be approximately10 % and is neglected in this study.

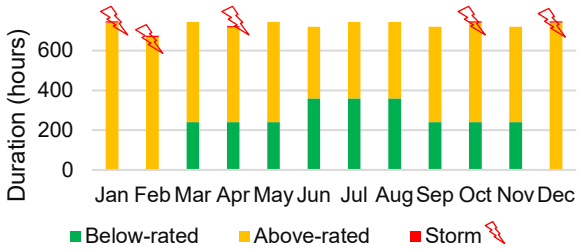


*Figure 3: Idealised yearly metocean conditions*

### *3.2 Seabed response and anchor capacity*

The seabed input parameters to *Ancmac* and $K^2M^2$ were selected to be representative of lightly over consolidated clay around a circular plate anchor embedded at a depth of approximately20 m. The selected seabed values are similar to those reported by O'Loughlin et al., (2020) and Zhou et al., (2020), with an initial undrained strength, $s_{u0}$ =80 kPa, coefficient of consolidation, $c_v$ = 6 m/s$^2$, and sensitivity, $S_t$ = 2.5, at the anchor point. When seabed hardening was enabled, both seabed softening and whole-life seabed strengthening effects were included in the analysis. The required anchor size was determined from running the whole-life simulation and setting a minimum factor of safety, FoS ≥ 1, where the FoS is the ratio of the static anchor capacity, $Q_s = N_c s_u A$ to $T_{max}$, to the maximum applied tension in each simulated month.

The different whole-life seabed responses with and without hardening enabled, are summarised in Figures 4. In the case where a conventional taut mooring was used to generate the input anchor loads, the damage imposed on the seabed increased significantly during the first year (Figure 4 (d)) and this corresponded to a decrease to the minimum through-life undrained strength, anchor capacity (Figure 4 (a), (b) ) during the whole-life simulation. The damage remained at a maximum, $D$=1, until year-5, when $D$ started to decrease as the seabed softening effects were eclipsed by consolidation and increases in hardening and undrained strength when hardening was enabled (Figure 4 (b) ,(c)). At year-5, the seabed strength recovered to $s_{u0}$ and subsequently increased to a final normalised value of 1.3$s_{u0}$ and initial anchor capacity, $Q_{s0}$. If hardening was not enabled, $s_u$, decreased and remained at 0.6 $s_{u0}$ and $Q_{s0}$ and larger anchors were required to achieve a FoS ≥ 1 to withstand the 1-in-50 year storm applied at 15 years. In the case where a LRD was incorporated in the mooring and hardening enabled, the final normalised

undrained strength and anchor capacities were similar to the case where conventional mooring case loads were applied (at ~1.6 $s_{u0}$ and $Q_{s0}$). This is a result of the smaller applied anchor loads, which resulted in less seabed damage and therefore smaller and more gradual changes in $s_u$ and $Q_s$, which are balanced by smaller increases in hardening over the design lifetime. When hardening was disabled, similar to in the conventional mooring case, $s_u$ and $Q_s$ decreased towards a minmum value of 0.6 $s_{u0}$ and $Q_{s0}$, and as a result a larger anchor was required and this contributed to a more gradual increase in damage over the design lifetime towards $D \rightarrow 1$.

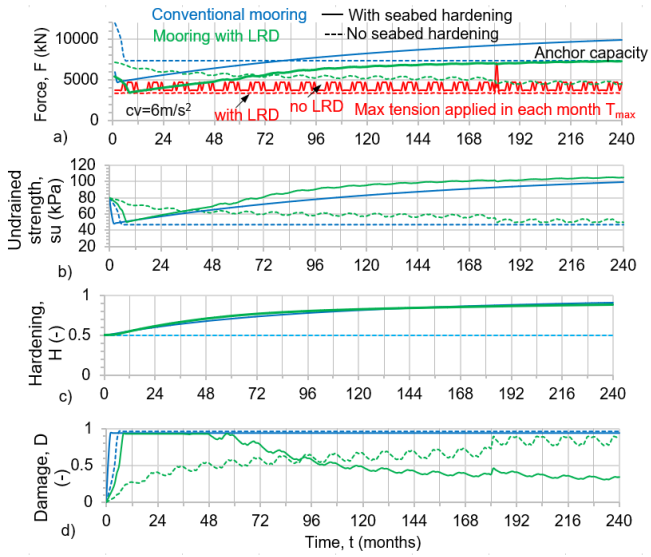


*Figure 4 Summary of seabed changes in (a) anchor capacity, (b) undrained strength, (c) hardening and (d) damage relative to applied tension loads*

Minimum required anchor sizes for a taut mooring with and without a LRD, and with and without seabed hardening enabled during the simulations are summarised in Table 4. Introducing LRDs into the taut mooring system reduces anchor size by 30% . This is a result of smaller loads being transmitted to the anchor. Separately including beneficial whole-life seabed hardening effects in the analysis reduces anchor size for both conventional taut mooring and mooring with LRD, by 37 and 30 % respectively. Finally, when both LRD and whole-life seabed effects are considered together, the minimum required anchor size is more than halved.

*Table 4: Comparison of minimum required anchor size*

| **Taut mooring case** | **Required anchor size, $A$ (m²)** | |
|---|---|---|
| | **No seabed hardening** | **With seabed hardening** |
| Conventional mooring | 11.9 | 7.5 |
| Mooring with LRD | 7.5 | 5.3 |

### *3.3 Limitations and future work*

To find the required anchor sizes summarised in Table 4, this study adopts a FoS limit on the static anchor capacity. This study does not consider movement of the anchor as the loads come from a mooring analysis where the anchor is represented as a fixed pin. Further design efficiencies could result from considering anchor ductility, where the anchor can move from its installed position and mobilise dynamic seabed effects such as added mass (Kwa et al., 2022; Kwa et al., 2023). This could have an effect on the mooring and connected floater responses and will be explored in future work.

## 4 CONCLUSIONS

This study presents an anchor macro model, which captures seabed response when coupled with a mooring-floater FEM. Results from an example whole-life application of the anchor-mooring-floater model demonstrate how it can be used to assess the through-life changes in seabed response and anchor capacity. Results show a possible 50 % decrease in the required anchor size from combining beneficial effects of LRDs in the mooring lines, and whole-life seabed strengthening effects, which is more than if either effect were considered separately. If dynamic anchor capacity were also considered and the anchor is permitted to move, rather than be treated as a fixed pin connection in mooring analyses, then this could also lead to further reductions in the required anchor size.

## 5 ACKNOWLEDGEMENTS

This work forms part of research supported by the Royal Academy of Engineering under the Research Fellowship Programme, RAEng Chair in Emerging Technologes Centre of Excellence in Intelligent & Resilient Ocean Engineering (IROE), and Supergen ORE Hub (Grant EPSRC EP/S000747/1). Katherine Kwa is supported by the RAEng Research Fellowship Scheme, David White is supported by the Supergen ORE Hub, Susan Gourvenec is supported by the Royal Academy of Engineering through the Chair in Emerging Technologies scheme, and Adam Sobey is supported by The Lloyd‘s Register Foundation.

## 6 REFERENCES

Allen, C. et al. (2020) Definition of the UMaine VolturnUS-S Reference Platform Developed for the IEA Wind 15MW Offshore Reference Wind Turbine. Golden, CO: National Renewable Energy Laboratory. NREL/TP-5000-76773.

Andersen, K.H. (2015). Cyclic soil parameters for offshore foundation design. Frontiers in offshore geotechnics III 5.

Bransby, M.F. (2002) The undrained inclined load capacity of shallow foundations after consolidation under vertical loads. In Num. Models in Geomech.: 8th Int. Symp. Rotterdam, Netherlands, Balkema.

Cassidy M.J. et al. 2012. A plasticity model to assess the keying of plate anchors. Géot., 62(9): 825–836.

Cocjin M., et al. (2014) Tolerably mobile subsea foundations –Observations of performance. Géot. 64(11): 895-909.

Deeks, A., et al. (2014) Design of direct on-seabed sliding foundations, OMAE2014-24393, V003T10A024.

DNV (2021). DNG-RP-E302: Recommended practices: design & installation of plate anchors in clay. DNV

Evan, G. et al. 2020. Definition of the IEA 15-Megawatt Offshore Reference Wind. Golden, CO: National Renewable Energy Laboratory. NREL/TP-5000-75698.

Gourvenec, S., et al. (2014). A method for predicting the consolidated undrained bearing capacity of shallow foundations. Géot., 64(3), pp.215-225.

Gourvenec, S. (2020) Whole-life geotechnical design: What is it? What's it for? So what? And what next? Proc. 4th Int. Symposium on Frontiers in Offshore Geotechnics, Austin, Texas, USA, Ed. Westgate, Z., ASCE Geo-Institute and DFI, ISBN: 978-0-9763229-4-8

Heath, J.E. et al. (2017). Applicability of geotechnical approaches & constitutive models for foundation analysis of marine renewable energy arrays. Renew. & Sust. Energy Reviews, 72, 191-204.

Houlsby, G.T. & Martin, C.M. (1992) Modelling of the behaviour of foundations of jack-up units on clay. Proc. Wroth Memorial Symp. Predictive Soil Mech., Oxford

Houlsby, G.T., & Wroth, C. P. (1991). The variation of shear modulus of a clay with pressure and overconsolidation ratio. Soils & Found., 31(3), 138-143.

Iwan, W.D. (1967). On a class of models for the yielding behavior of continuous & composite systems.

Jostad, H. P., et al. (2020). Evaluation of soil models for improved design of offshore wind turbine foundations in dense sand. Géot., 70(8), 682-699.

Kwa, K.A. et al. (2022) A numerical macro model to simulate the whole life response of anchors for floating offshore renewable energy systems. OMAE 2022-81101, V009T10A003 Hamburg, Germany.

Kwa, K.A., et al. (2021a). Analysis of the added mass term in soil bearing capacity problems. Géot. Lett., 11(1):.80-87.

Kwa, K.A., & White, D.J. (2021b). Enhanced anchoring systems for MRE infrastructure: 'whole life' soil-anchor-floating system interactions. 14th EWTEC, Plymouth, UK

Kwa, K.A., et al. (2023) The RSN-CSI model: A whole life geotechnical anchor macro model for floating offshore systems submitted to Applied Ocean Research

Martin, C.M. & Randolph, M. F. (2001). Applications of the lower & upper bound theorems of plasticity to collapse of circular foundations. 10th Int. Conf. Computer Methods and Advances in Geomech.

Martin, C.M. & Randolph, M. F. (2001). Applications of the lower & upper bound theorems of plasticity to collapse of circular foundations.10th Int. Conf. Computer Methods and Advances in Geomech.

Nova R. & Montrasio L. (1991) Settlements of shallow foundations on sand. Geot., 41(2): 243-256.

Neubecker, S.R. and Randolph, M.F. (1995). Profile and frictional capacity of embedded anchor chains. Journal of geotechnical engineering, 121(11), pp.797-803.

O'Loughlin, C.D., et al. (2017). Plate Anchors for Mooring Floating Facilities–A View Towards Unlocking Cost & Risk Benefits. In Offshore Site Investigation Geotech 8th Int. Conf. Proc, pp. 978-986).

O'Loughlin, C.D., et al. (2020). Load-controlled cyclic T-bar tests: a new method to assess effects of cyclic loading & consolidation Géot. Lett., 10(1), 7-15.

Peccin da Silva, A., et al. (2021). A non-associative macro-element model for vertical plate anchors in clay. Canadian Geo. J.

Randolph, M., (2004). Characterisation of soft sediments for offshore applications, Geotech & Geophys. Site Charac., Rotterdam.

Robertson, A.N., et al. (2020). OC6 Phase I: Investigating the underprediction of low-frequency hydrodynamic loads and responses of a floating wind turbine. In Journal of Physics: Conference Series (Vol. 1618, No. 3, p.032033).

Smith V.B. & White D.J. (2014) Volumetric hardening in axial pipe soil interaction. Offshore Tech. Conf. Asia, OTC ASIA 2014 (Vol. 2, pp.1611-1621).

Schotman, G.J.M. (1989). The effects of displacements on the stability of jackup spudcan foundations. 21st Offshore Tech. Conf., Houston, Texas, OTC 6026.

Stanier, S.A. & White, D.J., (2018). Enhancement of bearing capacity from consolidation: due to changing strength or failure mechanism?. Géot., 69(2), pp.166-173.

Tom, J.G., et al., 2019, June. Fluid-structure-soil interaction of a moored wave energy device. In International Conference on OMAE (Vol. 58899, p. V010T09A024). ASME

Verruijt, A. (1995). Computational geomechanics (Vol. 7). Springer Science & Business Media.

White, D.J., et al. (2021). A cyclic py model for the whole-life response of piles in soft clay. Computers & Geotechnics, 141, 104519.

Zhou, Z., et al. (2020). Improvements in plate anchor capacity due to cyclic and maintained loads combined with consolidation. Géot., 70(8), pp.732-749.